Electronic Supplementary Material (ESI) for ChemComm.
This journal is © The Royal Society of Chemistry 2023

# Experimental Section

### *Synthesis of Pd metallene*

All chemicals were used as received without further purification. Pd metallene were synthesized by a simple wet-chemistry strategy[1]. Briefly, 20 mg of $Pd(acac)_2$ and 0.25 g of trinoctylphosphine oxide (TOPO) were ultrasonically dissolved in octanoic acid (OA) and maintained at 60 °C in an oil bath. Then, 20 mg of $Mo(CO)_6$ and 5 mL of DMF were added into the above mixture and maintained for 1h. The black precipitates were collected by centrifugation and washed.

### *Electrochemical experiments*

Electrochemical measurements were performed on a CHI-660 electrochemical workstation (CHI-660E) in a three-electrode configuration, where carbon cloth (CC)-loaded catalyst (0.5 mg $cm^{-2}$), Ag/AgCl electrode and graphite rod were used as working, reference and counter electrodes, respectively. All potentials were referenced to reversible hydrogen electrode (RHE) by following equation: $E_{RHE}$ (V)=$E_{Ag/AgCl}$+0.198+0.059×pH. The electrocatalytic NORR measurements were performed in NO saturated 0.5 M $Na_2SO_4$ electrolyte using a gas-tight H-cell separated by a Nafion 211 membrane. The Nafion membrane was pretreated by boiling it in 5% $H_2O_2$ solution for 1 h, 0.5 M $H_2SO_4$ for 1 h and deionized water for 1 h in turn. Prior to NORR test, all the feeding gases were purified through two glass bubblers containing 4 M KOH solution and the cathodic compartment was purged with Ar for at least 30 min to remove residual oxygen. During each electrolysis, high-purity NO gas (99.9%) was continuously purged into the cathodic chamber at a flow rate of 20 mL $min^{-1}$. After electrolysis for 1 hour at the specified potential, water and gas products are detected by colorimetry and gas chromatography (GC, Shimadzu GC2010) respectively.

### *Determination of $NH_3$*

The generated $NH_3$ was determined by the indophenol blue method[2]. Generally, we took 0.5mL electrolyte from the electrochemical reaction vessel and dilute it 10 times with deionized water. Then we removed 2 mL of diluted solution into a clean

vessel followed by sequentially adding NaOH solution (2 mL, 1 M) containing $C_7H_6O_3$ (5 wt.%) and $C_6H_5Na_3O_7$ (5 wt.%), NaClO (1 mL, 0.05 M), and $C_5FeN_6Na_2O$ (0.2 mL, 1wt.%) aqueous solution. The mixed solution was subjected to UV-vis measurement using the absorbance at 655 nm wavelength, after the incubation for 2 h at room temperature. We calibrated the concentration-absorbance curves by the standard $NH_4Cl$ solution with a series of concentrations, and the $NH_3$ yield rate and Faradaic efficiency (FE) were calculated by the following equation[3]:

$$NH_3 \text{ yield} = (c \times V) / (17 \times t \times A) \quad (1)$$

Faradaic efficiency was determined by the following equation:

$$FE_{NH3} = (5 \times F \times c \times V) / (17 \times Q) \times 100\% \quad (2)$$

where $c$ (μg $mL^{-1}$) is the measured $NH_3$ concentration, $V$ (mL) is the volume of electrolyte in the cathode chamber, $t$ (s) is the electrolysis time and $A$ is the surface area of CC (1×1 $cm^2$), $F$ (96500 C $mol^{-1}$) is the Faraday constant, $Q$ (C) is the total quantity of applied electricity.

The detailed procedures for colorimetric determination $N_2H_4$ are provided in our previous publications[4]

***Characterizations***

X-ray diffraction (XRD) pattern was gathered on a Rigaku D/max 2400 diffractometer[5]. X-ray photoelectron spectroscopy (XPS) analysis was gathered on a PHI 5702 spectrometer. Atom force microscopy (AFM) was performed on a Nanoscope-IIIa scanning probe microscope. Transmission electron microscopy (TEM), high-resolution transmission electron microscopy (HRTEM) and selected area electron diffraction (SAED) were recorded on a Tecnai $G^2$ F20 microscope.

***Calculation details***

DFT calculations were performed using the Cambridge sequential total energy package (CASTEP) with projector augmented wave pseudopotentials. The Perdew-Burke-Ernzerhof (PBE) generalized gradient approximation (GGA) functional was used for the exchange-correlation potential. The van der Waals interaction was described by using the empirical correction in Grimme's scheme, i.e., DFT+D. The electron wave functions were expanded using plane waves with a cutoff energy of 450

eV, and a Monkhorst-Pack grid 3 × 3 × 1 was used for k-point sampling. Besides, the convergence thresholds of energy and forces were set to be $1 \times 10^{-5}$ eV and 0.02 eV $Å^{-1}$, respectively. Pd (111) was modeled by a 4 × 4 supercell, and a vacuum region of 10 Å was used to separate adjacent slabs.

The free energies (ΔG, 298 K) for each reaction were given after correction:

$$\Delta G = \Delta E + \Delta ZPE - T\Delta S \quad (3)$$

where $\Delta E$ is the adsorption energy, $\Delta ZPE$ is the zero-point energy difference and $T\Delta S$ is the entropy difference between the gas phase and adsorbed state.

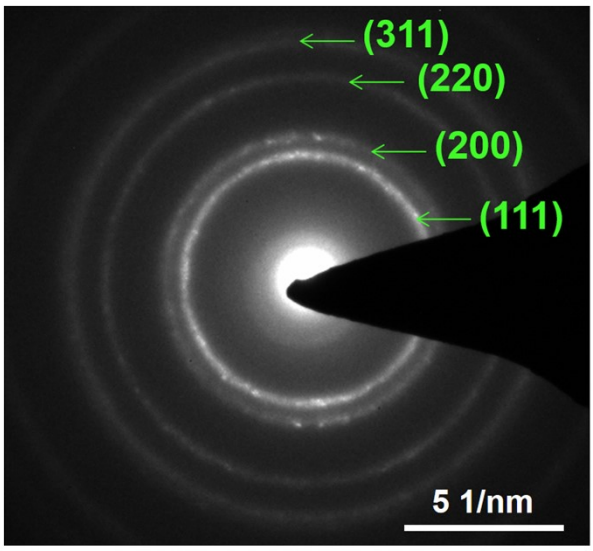


Fig. S1. SAED pattern of Pd metallene.

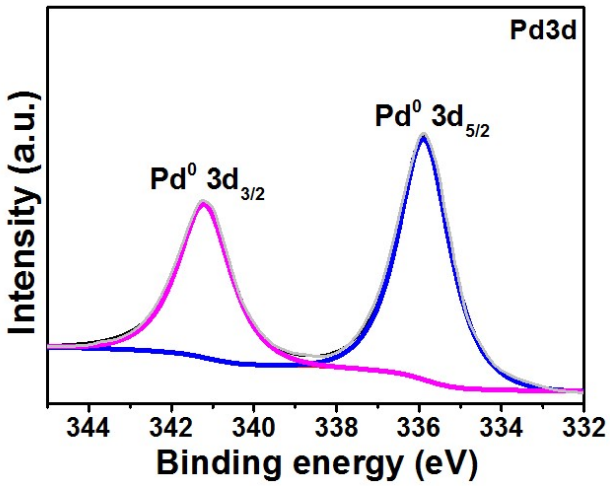

Fig. S2. XPS spectra of Pd3d spectrum.

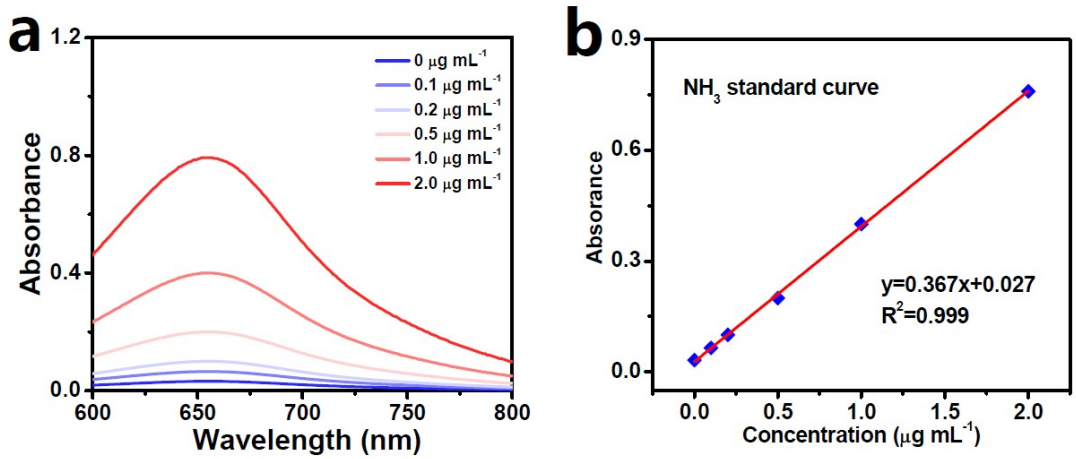


Fig. S3. (a) UV-vis absorption spectra of $NH_4^+$ assays after incubated for 2 h at ambient conditions. (b) Calibration curve used for the calculation of $NH_3$ concentrations.

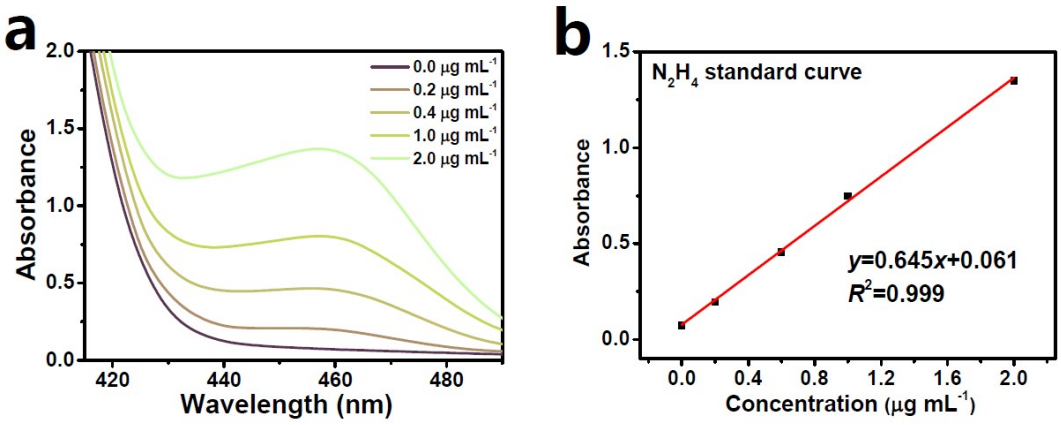


Fig. S4. (a) UV-vis absorption spectra of $N_2H_4$ assays after incubated for 20 min at ambient conditions. (b) Calibration curve used for calculation of $N_2H_4$ concentrations.

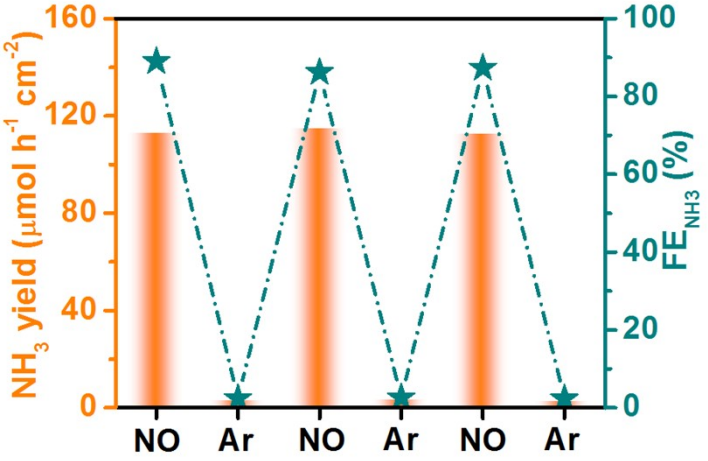

Fig. S5. NO/Ar switching experiment at -0.3 V.

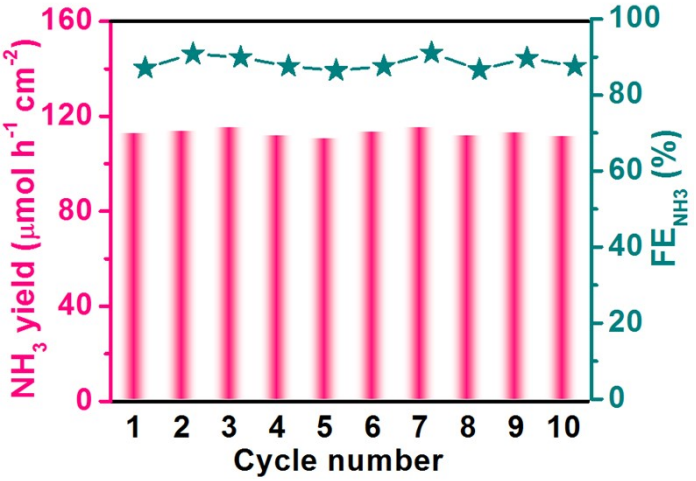


Fig. S6. Cycling test of Pd metallene at -0.3 V.

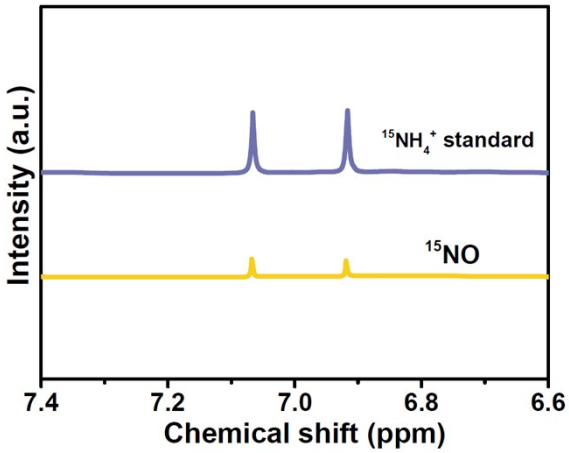


Fig. S7. $^{1}H$ NMR spectra of $^{15}NH_4^+$ standard sample and those fed by $^{15}NO$ and Ar after NORR electrolysis on Pd metallene at -0.3 V. The detailed procedure for NMR measurement was provided in our previous publication[6].

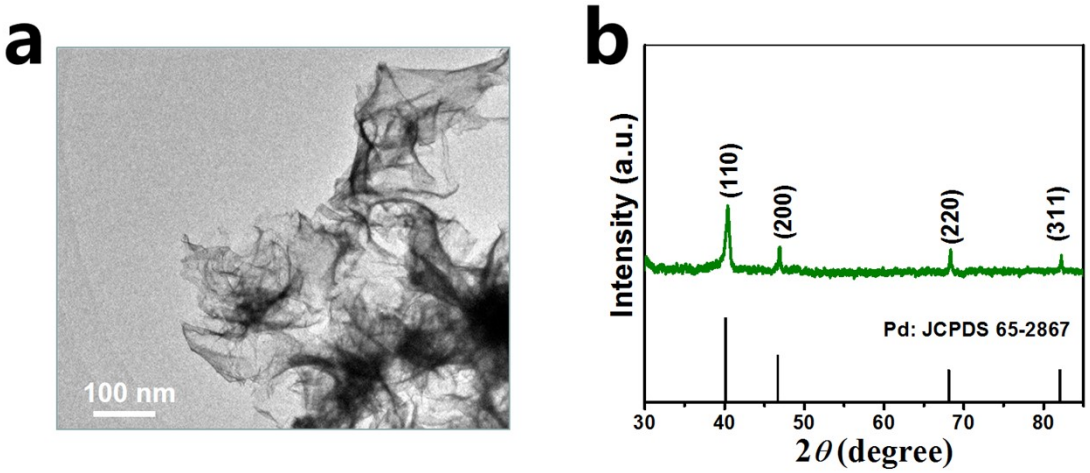


Fig. S8. (a) TEM image and (b) XRD pattern of Pd metallene after stability test.

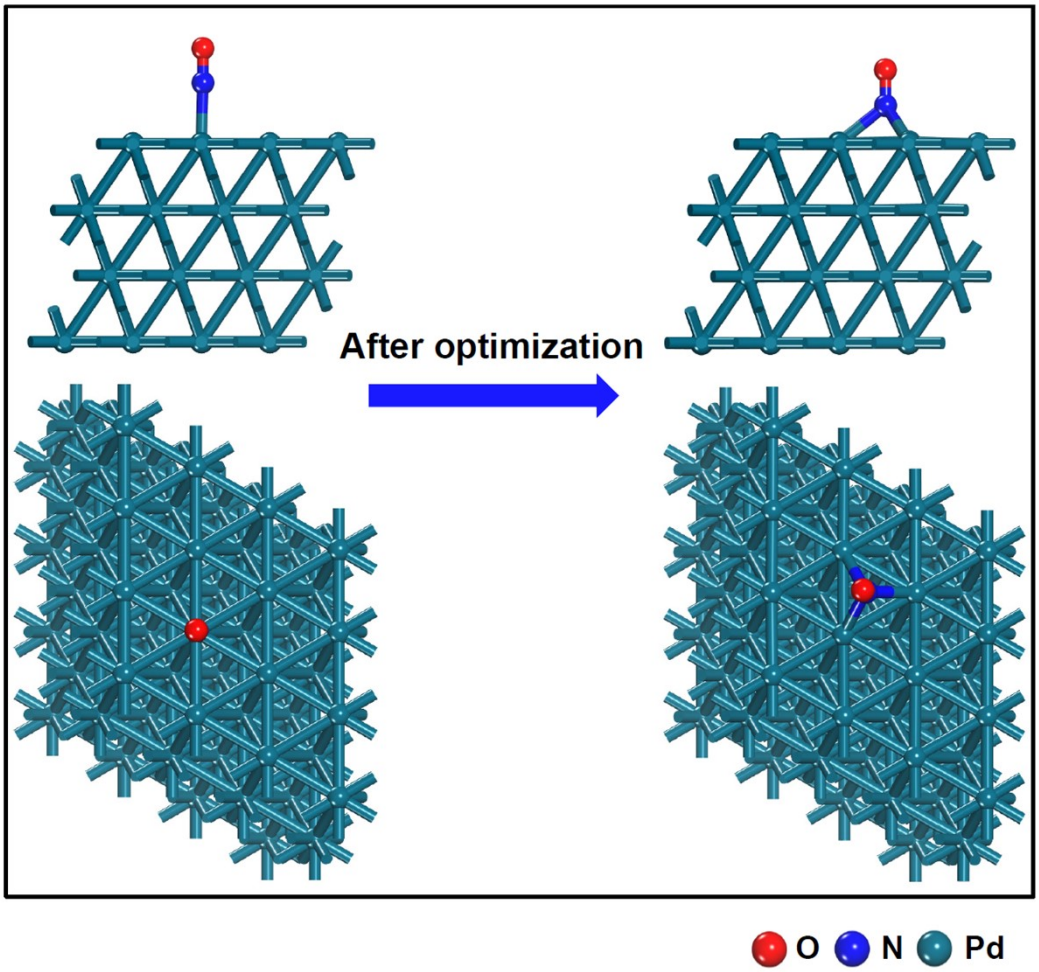


Fig. S9. The configuration of *NO on the top site of Pd before and after geometry optimization.

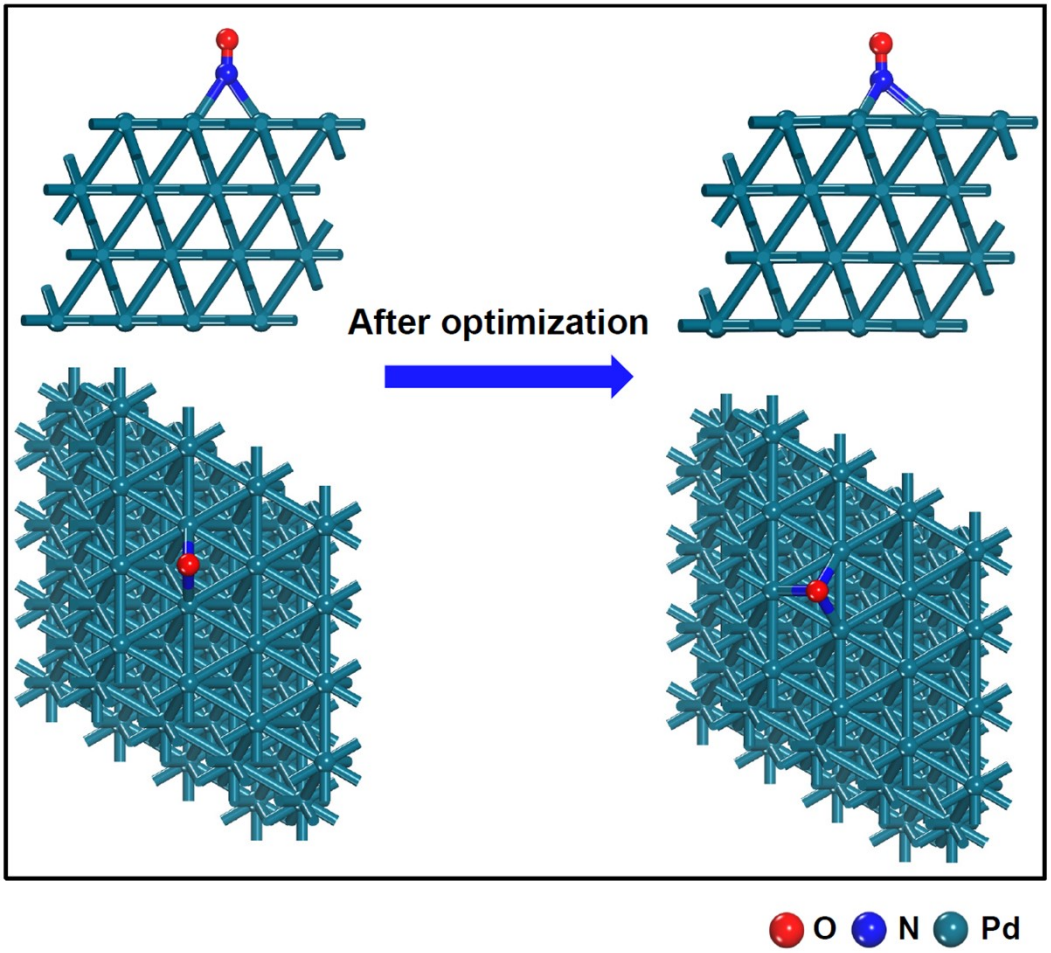


Fig. S10. The configuration of *NO on the bridge site of Pd before and after geometry optimization.

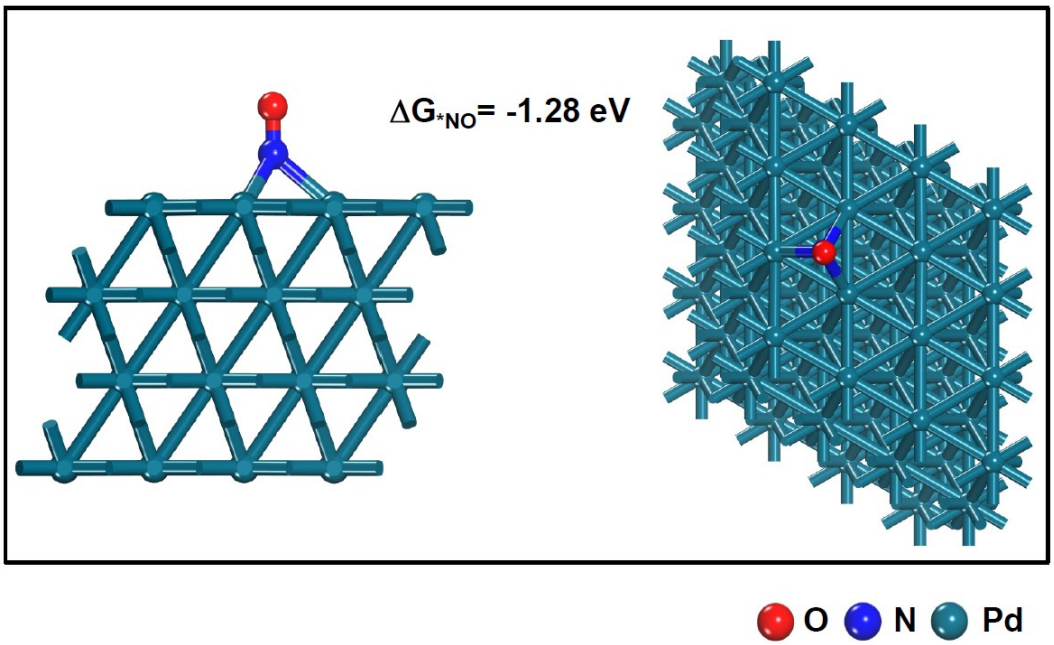


Fig. S11. The configuration of *NO on the fcc site of Pd after geometry optimization.

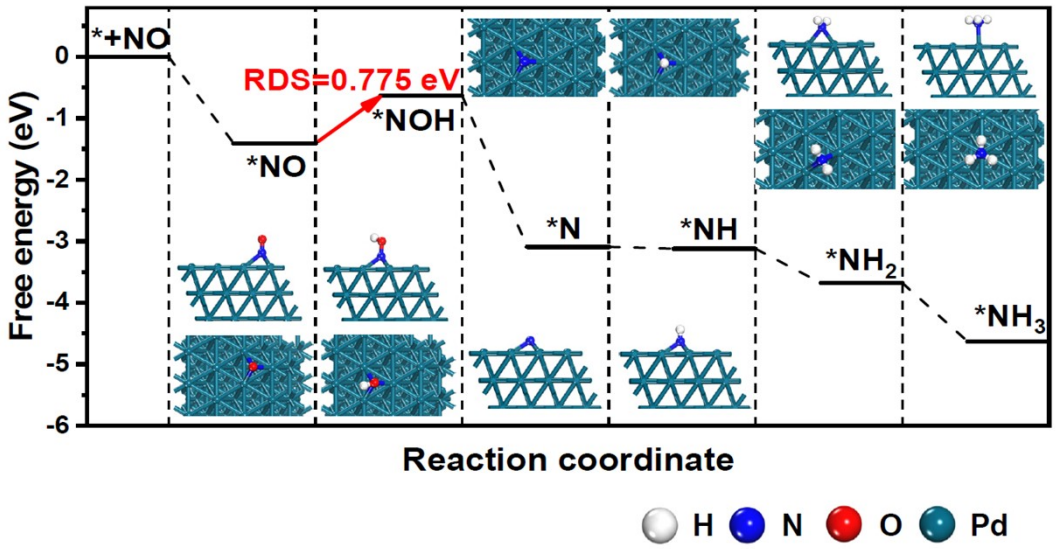


Fig. S12. Free energy diagram of the distal-O reaction pathway on hcp site of Pd and optimized configurations of NORR intermediates.

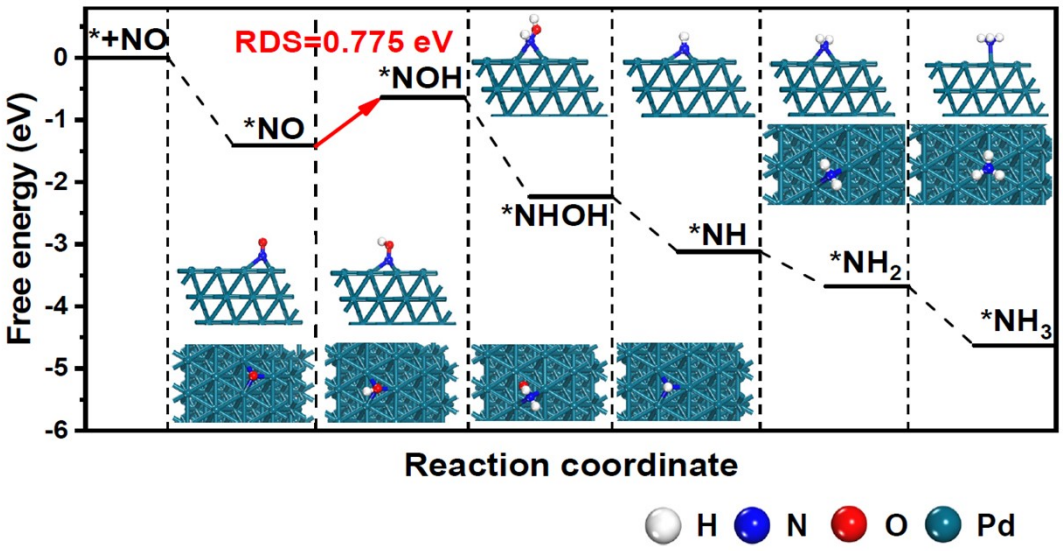


Fig. S13. Free energy diagram of the alternating-O reaction pathway on hcp site of Pd and optimized configurations of NORR intermediates.

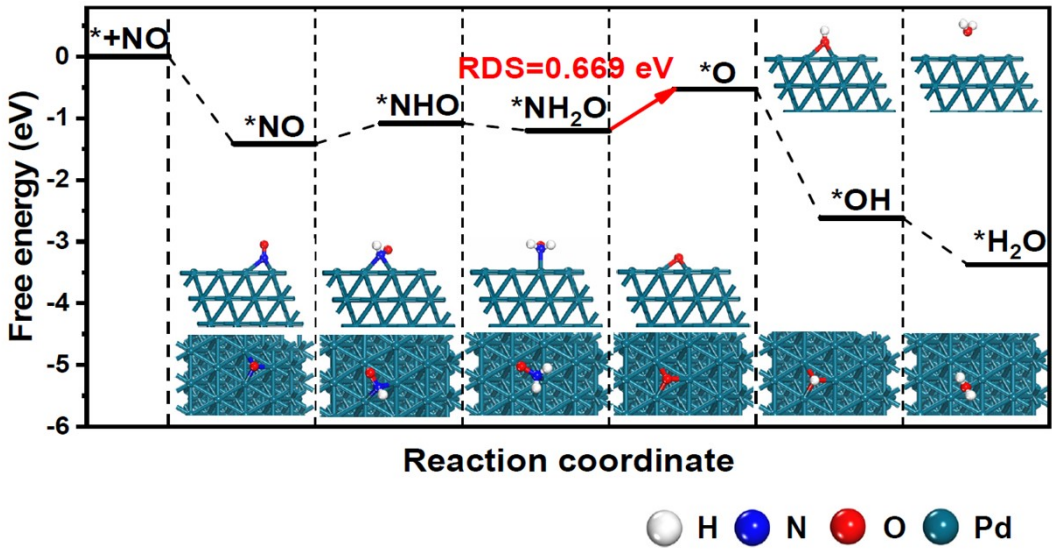


Fig. S14. Free energy diagram of the distal-N reaction pathway on hcp site of Pd and optimized configurations of NORR intermediates.

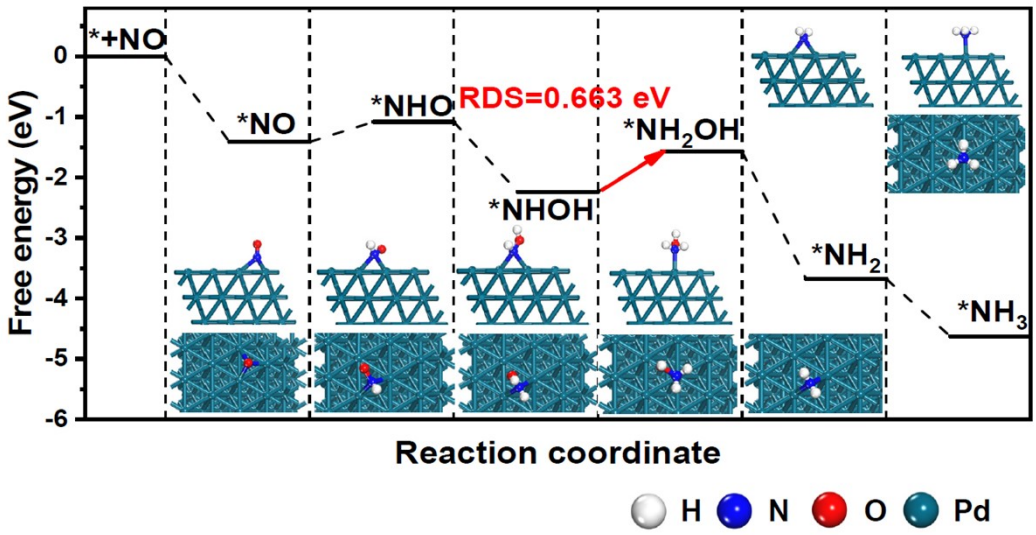


Fig. S15. Free energy diagram of the alternating-N reaction pathway on hcp site of Pd and optimized configurations of NORR intermediates.

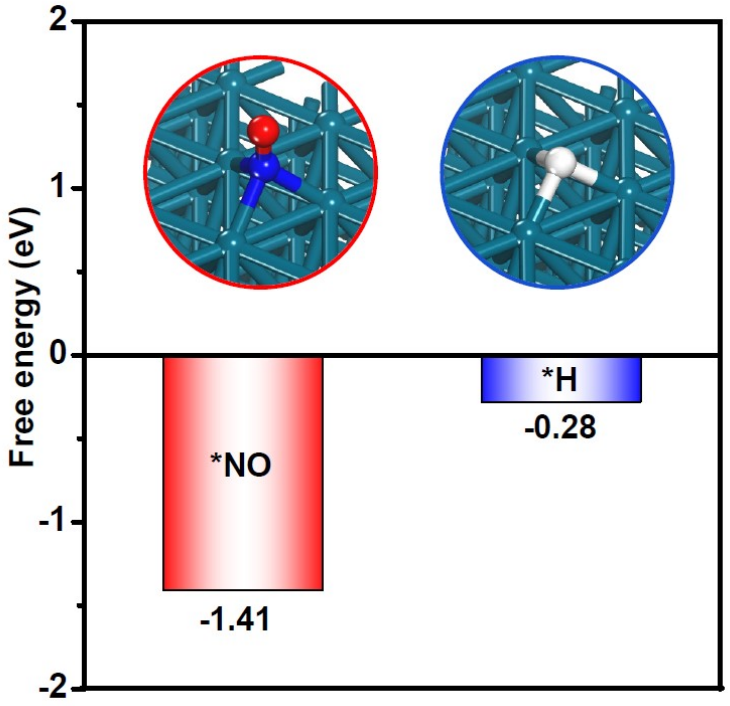


Fig. S16. Binding free energies of *NO and *H on hcp site of Pd.

Table S1. Comparison of optimum $NH_3$ yield and Faradic efficiency (FE) for recently reported state-of-the-art NORR electrocatalysts at ambient conditions.

| Catalyst | Electrolyte | $NH_3$ yield rate ($\mu mol\ h^{-1}\ cm^{-2}$) | FE (%) | Potential (V vs. RHE) | Ref. |
|---|---|---|---|---|---|
| $Mo_2C$ | 0.5 M $Na_2SO_4$ | 122.7 | 86.3 | -0.4 | [7] |
| $Ni_2P$/CP | 0.1 M HCl | 33.47 | 76.9 | -0.2 | [8] |
| $Ru_{0.05}Cu_{0.95}$ | 0.05 M $Na_2SO_4$ | 17.68 | 64.9 | -0.5 | [9] |
| $Cu_2O$@$CoMn_2O_4$ | 0.1 M $Na_2SO_4$ | 94.18 | 75.05 | -0.9 | [10] |
| NiO/TM | 0.1 M $Na_2SO_4$ | 125.3 | 90 | -0.6 | [11] |
| a-$B_{2.6}C$@$TiO_2$/Ti | 0.1 M $Na_2SO_4$ | 216.4 | 87.6 | -0.9 | [12] |
| FeP/CC | 0.2 M PBS | 85.62 | 88.49 | -0.2 | [13] |
| Bi NDs | 0.1 M $Na_2SO_4$ | 70.2 | 89.2 | -0.5 | [14] |
| CoP/TM | 0.2 M $Na_2SO_4$ | 47.22 | 88.3 | -0.2 | [15] |
| Ni@NC | 0.1 M HCl | 34.6 | 72.3 | 0.16 | [16] |
| **Pd metallene** | **0.5 M $Na_2SO_4$** | **112.5** | **89.6** | **-0.3** | **This Work** |

## Reference


[1]. X. Li, P. Shen, Y. Luo, Y. Li, Y. Guo, H. Zhang and K. Chu, *Angew. Chem. Int. Edit.*, 2022, **134**, e202205923.

[2]. N. B. Schmidt, J. D. Buckner, A. Pusser, K. Woolaway-Bickel, J. L. Preston and A. Norr, *Behavior Therapy*, 2012, **43**, 518-532.

[3]. C.-Z. He, Y.-X. Zhang, J. Wang and L. Fu, *Rare Metals*, 2022, **41**, 3456-3465.

[4]. Y. Luo, K. Chen, P. Shen, X. Li, X. Li, Y. Li and K. Chu, *J. Colloid Interf. Sci.*, 2023, **629**, 950-957.

[5]. J. Wu and Y.-X. Yu, *Int. J. Hydrogen Energy*, 2022.

[6]. X. Li, G. Zhang, P. Shen, X. Zhao and K. Chu, *Inorg. Chem. Front.*, 2023, **10**, 280-287.

[7]. K. Chen, P. Shen, N. Zhang, D. Ma and K. Chu, *Inorg. Chem.*, 2023, DOI: 10.1021/acs.inorgchem.2c03714.

[8]. T. Mou, J. Liang, Z. Ma, L. Zhang, Y. Lin, T. Li, Q. Liu, Y. Luo, Y. Liu, S. Gao, H. Zhao, A. M. Asiri, D. Ma and X. Sun, *J. Mater. Chem. A*, 2021, **9**, 24268-24275.

[9]. J. Shi, C. Wang, R. Yang, F. Chen, N. Meng, Y. Yu and B. Zhang, *Sci. China Chem.*, 2021, **64**, 1493-1497.

[10]. C. Bai, S. Fan, X. Li, Z. Niu, J. Wang, Z. Liu and D. Zhang, *Adv. Funct. Mater.*, 2022, **32**, 2205569.

[11]. P. Liu, J. Liang, J. Wang, L. Zhang, J. Li, L. Yue, Y. Ren, T. Li, Y. Luo, N. Li, B. Tang, Q. Liu, A. M. Asiri, Q. Kong and X. Sun, *Chem. Commun.*, 2021, **57**, 13562-13565.

[12]. J. Liang, P. Liu, Q. Li, T. Li, L. Yue, Y. Luo, Q. Liu, N. Li, B. Tang, A. A. Alshehri, I. Shakir, P. O. Agboola, C. Sun and X. Sun, *Angew. Chem. Int. Ed.*, 2022, **61**, e202202087.

[13]. J. Liang, Q. Zhou, T. Mou, H. Chen, L. Yue, Y. Luo, Q. Liu, M. S. Hamdy, A. A. Alshehri, F. Gong and X. Sun, *Nano Res.*, 2022, **15**, 4008-4013.

[14]. Y. Lin, J. Liang, H. Li, L. Zhang, T. Mou, T. Li, L. Yue, Y. Ji, Q. Liu, Y. Luo, N. Li, B. Tang, Q. Wu, M. S. Hamdy, D. Ma and X. Sun, *Mater. Today Phys.*, 2022, **22**.

[15]. J. Liang, W.-F. Hu, B. Song, T. Mou, L. Zhang, Y. Luo, Q. Liu, A. A. Alshehri, M. S. Hamdy, L.-M. Yang and X. Sun, *Inorg. Chem. Front.*, 2022, **9**, 1366-1372.

[16]. S. Sethuram Markandaraj, T. Muthusamy and S. Shanmugam, *J. Adv. Sci*, 2022, **9**, 2201410.